2014 International Conference on Unmanned Aircraft Systems (ICUAS)
May 27-30, 2014. Orlando, FL, USA

Pitch Control of an Oblique Active Tilting Bi-rotor

Charles Blouin
Dep. of Mechancal Engineering
University of Ottawa
Ottawa, Canada
K1N 6N5
Email: cblou045@uottawa.ca

Eric Lanteigne
Dep. of Mechancal Engineering
University of Ottawa
Ottawa, Canada
K1N 6N5
Email: Eric.Lanteigne@uottawa.ca

***Abstract*—This article presents the design and pitch control of an Oblique Active Tiling (OAT) fixed-pitch bi-rotor. The oblique arms of the bi-rotor allow faster pitch response due to gyroscopic torque, compared to other vertical take-off designs. The effect of the design parameters on flight are analyzed to provide general guidelines for the design of OAT bi-rotors. The non-linear model of a bi-rotor is simulated in Matlab and a simplified controller is implemented on a small scale model.**

I. Introduction

Quadcopters have been the subject of numerous academic studies in recent years. Their low cost makes them ideal for aerial photography, search and rescue, mapping, and inspection [1]. Other rotor configurations were investigated for increased manoeuvrability of the vehicle. Tricopters have a faster yaw response, but require at least one servo-motor. They can also be fully actuated (move and rotate in all directions) when all their arms rotate as studied by [2] and [3]. Researchers and hobbyists tried various configurations such as coaxial-quadcopters [4], variable pitch quadcopters [5], [6], and reversing motors quadcopters[7]. A larger number of rotors, such as in a hexacopter or octocopter, is used for lifting a heavy payload, as well as for added safety in case of propulsion failures.

Large propellers are, in general, more efficient. Helicopters, while being the most efficient vertical take-off vehicle, have a swash plate, and are more complex than quadcopter designs. A two-propeller design can be a good compromise of efficiency versus mechanical complexity. [8] proposed an asymmetric design of a hexacopter with two larger propellers for higher efficiency and four smaller propellers for control. A "triquad", which is a combination of a helicopter and a tricopter, was built and studied [9]. The authors claim the efficiency of a helicopter without the swash plate complexity. With only two rotors, there are coaxial models [10] and non-coaxial (tilt rotor) models.

Tilt-rotor helicopters can be Forward-Aft active tilting (FAAT) or Oblique Active tilting (OAT). The OAT type has received very little attention from the research community at the time of writing. The former, with the tilt axis of the rotor intersecting the center of gravity (CG), were studied experimentally in 2002 by [11]. Tilt axis vehicles offer faster pitch and yaw responses than quadcopters while being simpler mechanically than a helicopter swash plate. In 2006, [12] developped a backstepping controller for a tilt-rotor using both lateral and longitudinal tilting of the rotors. In 2011, [13] studied a FAAT bi-rotor with a PID controller.

The following paper will present the model and dynamics of the OAT bi-rotor, the transformation of torques and forces to servo angles and motor commands, and the controller design. The controller is then simulated and a test vehicle, shown in Fig.1, is presented.

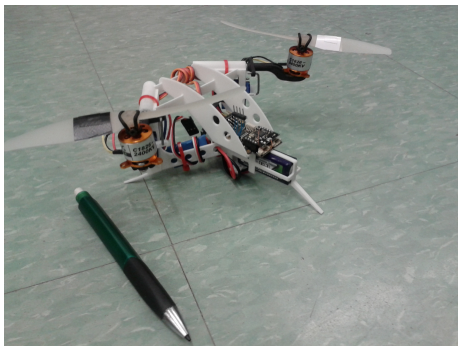

Fig. 1: Experimental model used to test the controller

This article is divided in the following manner: Section II is dedicated to the linear and non-linear models of an OAT bi-rotor. Section III is about the controller design and the simulation results. Section IV presents the physical model and the experimental results. Section V concludes the paper with a summary of the results and the key findings.

II. Description of Bicopters

Fixed pitch bi-rotors are made of five rigid bodies: the left and right propellers, the left and right servo-motor assemblies, and the main body. As shown in fig. 2, these parts are mechanically constrained and the frame will be assumed to be a rigid body. The bi-rotor has four control inputs: two motors that can vary their speed and two arms that can rotate due to the servo-motors.

The bi-rotor creates a pitch motion via two processes. When both arms pitch in the same direction, the thrust force is not in line with the CG. Thus, a torque is created that pitches the bi-rotor. Secondly, when the arms are pitching, they have a velocity, $\vec{\Omega}_l$ and $\vec{\Omega}_r$. The propellers and rotors have a certain angular momentum proportional to $\vec{\omega}_l$ and $\vec{\omega}_r$. Thus, a torque, perpendicular to the vectors $\vec{\Omega}$ and $\vec{\omega}$,

978-1-4799-2376-2/14/$31.00 ©2014 IEEE

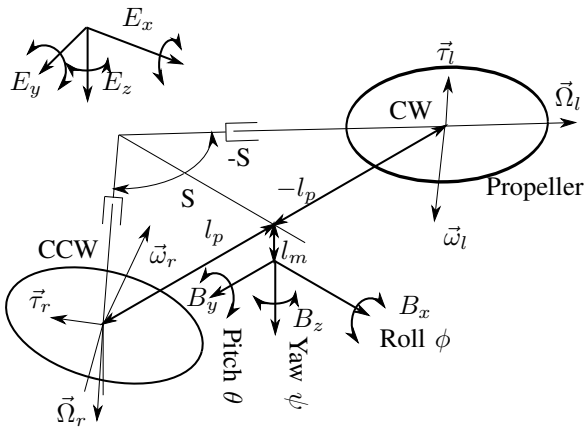

Fig. 2: Axis convention for an OAT, shown pitching forward

Fig. 3: Goddard and his liquid fuel rocket. Note that the gas exhaust at the top is over the liquid fuel and oxygen tanks. This design is no more stable than having the exhaust at the bottom. (NASA, Public Domain)

is generated. When the gyroscopic torque from the left and right propellers are added, they create a pitching motion. Consequently, the bi-rotor reacts faster than quadcopters as the pitching acceleration is proportional to both the rotors' angle and their angular rate. When the two arms pitch forward, the bi-rotor also pitches forward due to the gyroscopic torques τ_l and τ_r. Note that no roll moment is generated if the propellers' speed are the same ($|\vec{\omega}_l| = |\vec{\omega}_r|$) and the arms' rotational velocity are the same ($|\vec{\Omega}_l| = |\vec{\Omega}_r|$), since the two roll components of the gyroscopic torques are opposite.

A. Modeling

The bi-rotor is modeled as a set of non-linear differential equations, which is similar to the tilt rotor in [13]. However, the equations and the controllers are modified to include the swept angle of the arms. Thus, the gyroscopic torque will not have a negligible effect. Also, a "weight torque" is not included, although its incorrect inclusion can be found in other studies on bi-rotors.

It is a common misconception that bi-rotors act as a pendulum, as if they were hanging from the propellers. In reality, the weight is applied at the center of gravity; it will not cause the vehicle to maintain its vertical orientation. Consequently, gravity has no impact on the roll dynamic. This mistake can be found in the literature on bi-rotors in the form of a gravity torque. It is referred to as "rocket pendulum fallacy", from the design, seen in Fig. 3, of professor and physicist Robert Goddard, also considered the father of modern rocketry.

It can be shown experimentally, and using Newton's mechanics, that a bi-rotor has no gravity restoring torque. The thrust from the propeller is simply a force fixed in the frame of reference of the body. Fig. 4 shows the free body diagrams of the correct and incorrect models.

The model will follow the aeronautic axis convention with the body frame of reference $\mathbf{B} = \{\mathbf{B_x}, \mathbf{B_y}, \mathbf{B_z}\}$ and an inertial frame of reference $\mathbf{E} = \{\mathbf{E_x}, \mathbf{E_y}, \mathbf{E_z}\}$, centered

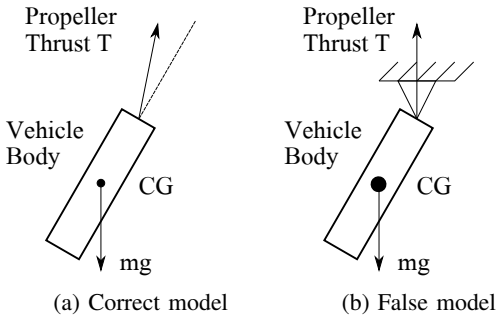

(a) Correct model (b) False model

Fig. 4: 2D model of the propeller thrust of a bi-rotor.

at the CG of the bi-rotor, as shown in Fig. 2. The frames of reference will be represented by the superscript b for the body frame of reference and e for the global inertial frame of reference. The position of the vehicle is $\mathbf{q^e} = [p^e\ \xi]^T$, where $\mathbf{q} = [x\ y\ z]$, and $\xi = [\phi\ \theta\ \psi]$. The right and left motors are positioned at $\mathbf{d_r^b}$ and $\mathbf{d_l^b}$. The value of $\mathbf{d_l^b}$ is $[0\ l_p\ l_m]$ and $\mathbf{d_r^b}$ is $[0\ -l_p\ l_m]$. To transform a vector from the body frame to the inertial frame, the following transformation is used, which respect the roll-pitch-yaw convention:

$$\mathbf{p^e} + R_b^e(\phi, \theta, \psi)\mathbf{d^b} \tag{1}$$

$$R_b^e = \begin{bmatrix} c_\theta c_\psi & s_\psi c_\theta & -s_\theta \\ c_\psi s_\theta s_\phi - s_\psi c_\phi & s_\psi s_\theta s_\phi + c_\psi c_\phi & c_\theta s_\phi \\ c_\phi s_\theta c_\psi + s_\psi s_\phi & s_\psi s_\theta c_\phi - c_\psi s_\phi & c_\theta c_\phi \end{bmatrix} \tag{2}$$

In the previous equations, $\mathbf{d^b}$ is a vector in the bi-rotor frame of reference and R_b^i is the orientation of the aircraft. See [14] for details on position description. The left motor, for example, is situated at $\mathbf{p_l^i} + R_b^i(\psi, \theta, \phi)\mathbf{d_r^b}$ in the inertial

frame of reference, where $R_b^i(\psi, \theta, \phi)$ is the rotation matrix from the body reference frame to the inertial reference frame. To cancel inertial forces (other than torque) from the motor on the bi-rotor when turning the motor and propeller assembly, the CG of the motor is placed along the axis of rotation of the arms. The velocity of the rotor is represented by the vector $\vec{\omega}$. When hovering, the relationship between the motor thrust $\mathbf{T}$ and the propeller speed is linearised around the hovering point as $\mathbf{T}(\vec{\omega}) = k\vec{\omega}$. In reality, the thrust is better modelled as $\mathbf{T}(\vec{\omega}) = k'\vec{\omega}\cdot|\vec{\omega}|$, but the linearisation can be used around hovering point [13][15]. For a more complete thrust dynamic, see [16]. Due to the symmetry along the axes of the bi-rotor, the inertia matrix of the bi-rotor is symmetrical. The I in Eq.(3) is the inertia of the whole assembly, neglecting small changes due to arm rotation.

$$I = \begin{bmatrix} I_{xx} & 0 & 0 \\ 0 & I_{yy} & 0 \\ 0 & 0 & I_{zz} \end{bmatrix} \tag{3}$$

The vector representing the velocity of the right propeller is $\vec{\omega_r}$ in the body frame. This vector is function of the swept angle S and the arm angle Ω.

$$\vec{\omega}_r = |\vec{\omega}_r| \begin{bmatrix} \cos S \sin \Omega \\ \sin S \sin \Omega \\ \cos \Omega \end{bmatrix} \tag{4}$$

The left arm angle is represented by $|\vec{\Omega}_l|$ in the body frame of reference. The arm orientation is represented by the vector $\vec{\Omega}$.

$$\vec{\Omega}_r = |\vec{\Omega}_r| \begin{bmatrix} \sin S \\ \cos S \\ 0 \end{bmatrix} \tag{5}$$

Four types of torque are acting on the vehicle from the arm. The thrust force, the gyroscopic force from the rotating propeller, the inertia force from rotating the arm assembly and the drag torque from the propellers. The moment $\vec{\tau_l}$ acting on the bi-rotor from the left propeller is given by:

$$\vec{\tau_l} = k\vec{\omega_l} \times \vec{d_l} + I_{prop}\dot{\vec{\Omega}}_l \times \vec{\omega}_l + I_{prop}\ddot{\vec{\Omega}}_l + k_p\vec{\omega_l} \tag{6}$$

The linearised torque resulting from the propeller drag is represented by the term $k_p\vec{\omega_l}$ in Eq.(6). This torque will be neglected for the controller analysis since both propellers are spinning at approximately the same speed in opposite direction when hovering. Also, when the vehicle is moving, a torque can arise from aerodynamic forces, which are also neglected. The derivation of the torques and positions related to the left arm is similar to the derivation for the right arm, but with a swept angle of $-S$. The direction of rotation of the rotor is also opposite.

There are three forces considered to affect the bi-rotor: the gravity $\vec{g}$ and the thrust from the two rotors: T_l^b and T_r^b. Aerodynamic forces are neglected since the small model is intended to operate at low speeds. An aerodynamic term of the form $\mathbf{F_d} = -1/2\rho\mathbf{v}|\mathbf{v}|AC_d$ could be added, where $\mathbf{v}$ is the vehicle velocity, A is its area, C_d the drag coefficient, and ρ the density of air. The drag force would be parallel to the incoming air flow. At high speeds, lift could be generated from wings, if any are present. Moreover, since the center of drag and the center of mass are not the same, an aerodynamic torque appears. The equations of motion neglecting the aerodynamic term take the following form:

$$m\ddot{p}^e = R_b^i(T_l^b + T_r^b) + m\vec{g^e} \tag{7}$$

$$\begin{bmatrix} \ddot{x} \\ \ddot{y} \\ \ddot{z} \end{bmatrix} = \frac{k}{m}\left(|\vec{\omega_r}| \begin{bmatrix} \cos S \sin \Omega_r \\ \sin S \sin \Omega_r \\ \cos \Omega_r \end{bmatrix} + |\vec{\omega_l}| \begin{bmatrix} \cos S \sin \Omega_l \\ -\sin S \sin \Omega_l \\ \cos \Omega_l \end{bmatrix} \right) + \vec{g^b} \tag{8}$$

B. Roll, yaw and linearisation

This section will demonstrate that a bi-rotor has characteristics very similar to a quadcopter for the roll dynamic and to a tricopter for the yaw dynamic. Thus, controllers developed for quadcopters and tricopters can be used to control the roll and yaw of bi-rotors. By expanding (6), we obtain the following for the roll dynamic for the left arm:

$$\begin{aligned} \tau_{l,x} =& k|\vec{\omega_l}|(\sin S \sin \Omega_l d_{l,z} - \cos \Omega_l)d_{l,y} \\ &+ \dot{\Omega}_l \cos(S) I_{zzp}\omega_l \\ &- \ddot{\Omega}_l \sin(S) I_{zza} \end{aligned} \tag{9}$$

During hover, the term $d_{l,z} \sin \Omega_l$ is small and can be neglected for linearization, and $\cos \Omega_l = 1$. Also, when the vehicle rolls and is stable in pitch and yaw, the arm parameters are $\dot{\Omega}_l = \dot{\Omega}_r = 0$ and $\ddot{\Omega}_l = \ddot{\Omega}_r = 0$. Thus, the total roll torque linearized around hover for the bi-rotor is:

$$\tau_{l,x} + \tau_{r,x} = k|\vec{\omega_l}||\mathbf{d_{l,y}}| + k|\vec{\omega_r}||\mathbf{d_{r,y}}| \tag{10}$$

Since k is assumed constant and $\mathbf{d_{l,y}}, -\mathbf{d_{r,y}}$ are equal, the equation of motion is given by:

$$\ddot{\phi} = \frac{2k|\mathbf{d_{r,y}}|}{I_{xx}}(|\vec{\omega_l}| - |\vec{\omega_r}|) \tag{11}$$

The difference $|\vec{\omega_l}| - |\vec{\omega_r}|$ can be written ω_d. Consequently, the transfer function is the following second order system:

$$\frac{\phi(s)}{\vec{\omega}_d(s)} = \frac{2k|\mathbf{d_{r,y}}|}{I_{xx}} \frac{1}{s^2} \tag{12}$$

As mentioned earlier, since the roll dynamic has a second order transfer function, it is very similar to the roll dynamic of a quadcopter, which is thoroughly studied in the literature.

By expanding (6), we obtain the following yaw torque

$$\vec{\tau_z} = k|\vec{\omega_l}| \cos S \sin \Omega_l |\mathbf{d_{l,y}}| + k|\vec{\omega_r}| \cos S \sin \Omega_r |\mathbf{d_{r,y}}| \tag{13}$$

During hover, $|\vec{\omega_l}| = |\vec{\omega_r}| = \omega$ to prevent any roll torque. For small angles, $\sin \Omega = \Omega$. Thus:

$$I_{xx}\ddot{\psi} = 2k\omega|\mathbf{d_{r,y}}|(|\Omega_r| - |\Omega_l|) \tag{14}$$

With $|\Omega_r| - |\Omega_l| = \Omega_d$, the transfer function is:

$$\frac{\psi(s)}{\Omega_d(s)} = \frac{2k\omega|\mathbf{d_{r,y}}|}{I_{xx}s^2} \tag{15}$$

Thus, the yaw control is a second order system, similar to a quad or tri-copter. However, unlike quadcopters, the applied torque is a function of the servo angle, not the propeller drag torque. Since servos respond faster than motors, bi-rotors will have a faster yaw response than quadcopters.

C. Pitch study and linearisation

The pitch moment from the left arm applied on the main body is:

$$\begin{aligned}\tau_{l,y} = &-\sin\Omega_l \cdot k|\vec{\omega_l}|(\cos S|\mathbf{d_{l,z}}|) \\ &+ (\dot{\Omega}_l \sin S \cos\Omega_l)|\vec{\omega_l}| \cdot I_{zzp} \\ &- (\ddot{\Omega}_l \cos S + \ddot{\theta}) \cdot I_{yya}\end{aligned} \tag{16}$$

From (17), we conclude that a swept angle of 0 (arm axis of rotation parallel to the roll axis) would remove the term proportional to $\vec{\Omega}$. Although the vehicle would be theoretically controllable, the range of Ω is limited in practice since the thrust has to keep pointing upward. Therefore, a swept angle of 0 is not usable. Another special case is a FAAT, with a swept angle of 90°, as studied by [13]. The term proportional to $\dot{\vec{\Omega}}$ equals 0. This term can be desirable because it can increase the controllability of the pitch of the bi-rotor.

To study the pitch, the tilt-rotor dynamics will be simplified to a 1D model, where the yaw and roll are stable and both arms have the same angle $\vec{\Omega}$. Using a small angle approximation, where $\sin x = x$ and $\cos x = 1$, the equation for the pitch becomes:

$$\begin{aligned}\frac{\ddot{\theta} I_{yy}}{2} = \tau_{l,y} = &-\Omega_l \cdot k|\vec{\omega}|(\cos S|\mathbf{d_{l,z}}|) \\ &+ (\dot{\Omega}\sin S)|\vec{\omega_l}| \cdot I_{zzp} \\ &- (\ddot{\Omega}\cos S + \ddot{\theta}) \cdot I_{yya}\end{aligned} \tag{17}$$

During hover, $|\vec{\omega}|$ can be assumed constant. Since the center of gravity is under the arms axis, and z is pointing downward, d_z is negative. The problem can then be simplified as

$$B(s) = d\ddot{\theta} = -a\ddot{\Omega} + b\dot{\Omega} + c\Omega \tag{18}$$

Where $a, \dots d$ are positive real numbers by design. In the FAAT design, the term $b\dot{\Omega}$ is zero when both arms are rotating at the same velocity. By designing the b constant to be positive, which means choosing the right propeller spinning direction, it is possible to apply a higher pitch torque on the bi-rotor. If the propellers are reversed, the gyroscopic torque will provide a negative feedback. The propeller orientation chosen is shown in Fig. 5.

One could imagine a configuration where the center of gravity is over the arm axis, such as in Fig. 6. This configuration was also investigated. The attitude controller would not change; the bi-rotor is not an inverted pendulum and it does not hang from the propeller. However, this configuration is not ideal for position control. A forward pitch will create a force opposed to the desired forward movement. Position control would still be possible, but it would be slower with the center of gravity over the arm

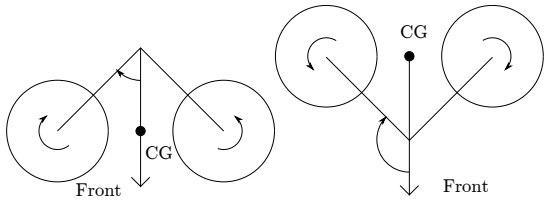

(a) $S \leq \pi/2$ (b) $S \geq \pi/2$

Fig. 5: Propeller direction for positive and negative swept angle and the CG under the arms

axis. Therefore, a configuration with the center of gravity of the bi-rotor under the axis of rotation of the arms will be studied.

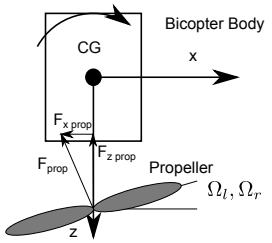

Fig. 6: Side view of a bi-rotor with the propellers under the center of gravity.

The linear model of the bi-rotor pitch dynamic is studied with its transfer function:

$$B(s) = \frac{\theta(s)}{\Omega(s)} = \frac{-as^2 + bs + c}{ds^2} \tag{19}$$

The negative term as^2 is a negative feedback from the arm's inertia. Although measurement techniques are available for servo characteristics, they require precise calibrations [17]. Often, only the reaction speed from the manufacturer R_t is given. It was assumed that this reaction time is equal to two time constants, which means that the arm would reach 86% of its final position in a time R_t. Consequently, the servo was approximated as a first order system and in the non-linear model, a saturation was added. The transfer function of the servo is the following:

$$S(s) = \frac{\Omega(s)}{\Omega_d(s)} \frac{1}{R_t/2s + 1} \tag{20}$$

III. Controller study

Two controllers were compared and tested in simulation and experimentally. A PD controller is often implemented for its simplicity and good performance, as in [13]. The implementation is fast on micro-controllers and it can be tuned using LQR, Ziegler-Nichols method or with manual tuning. For each controller, two simulations were performed: the first used the linearized model while the second used the complete non-linear model. The non-linear simulation includes a discrete time-step and gyroscopic noise. The gyroscopic sensor noise is modeled as Gaussian noise. Finally, the stability of the controllers is evaluated by checking the

frequency response to disturbances in the pitch axis of the controlled bi-rotor.

The non-linear model is simulated in Simulink. The step inputs given to the bicopter will be of 0.5 rad for the non-linear model and 1 rad for the linear model. Fig. 7 shows a block diagram of the pitch simulation. It includes the gaussian noise from the gyroscope reading, the saturation of the servo speed and external disturbances coming from vibrations or aerodynamic torques. The block $B(s)$ represents the non-linear model of the bicopter's pitch as described in Eq.17 while $S(s)$ is the servo model as described in Eq.20.

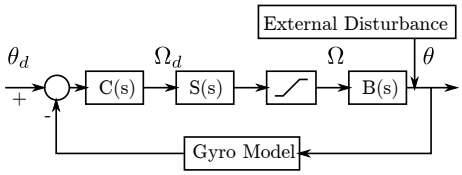

Fig. 7: Pitch control block diagram

Table I shows the constants used for the simulation. They are based on the physical model built and presented in the next section. The inertia constants were obtained using the CAD model. The objective is to design a controller

TABLE I: Physical parameters of the bi-rotor

Parameter	Value	Unit
R_t	0.14	s
Gyro noise (std. dev.)	8.7×10^{-4}	rad
l_m	0.02	m
S	45	degree
I_{zzp}	5.37×10^{-6}	kg×m^2
I_{zza}	1.5×10^{-6}	kg×m^2
I_{zzb}	6.44×10^{-5}	kg×m^2
$\lvert\vec{\omega}\rvert$	1466	rad/s
Servo max. rate	7.46	rad/s

for human piloting. Therefore, considering the size of the device, the parameters are a rise time of 0.15 seconds, low steady state error and an overshoot under 10 % for a step input in position of 0.5 rad or 28.6 degree.

A. OAT and FAAT comparison with a PD controller

First, OAT and FAAT types were compared in simulation. The model simulated for each type is the same with the exception of the swept angle: it is 0 for the FAAT. The results are shown in Fig. 8 for a PD controller. The parameters of the controller are $P = 0.07$ and $D = 0.01$ for the OAT and $P = 0.02$ and $D = 0.01$ for the FAAT. The results clearly demonstrate the slower pitch response of the FAAT. A lower P constant has to be used for the FAAT or the system diverges. Consequently, for a vehicle mostly hovering, an OAT design is advantageous for its faster pitch response. The rest of the analysis will be done on the OAT design. The PD controller was tuned to meet the design criteria. The results of the linear simulation, seen in Fig. 9, diverge significantly from the results of the simulation of the controller applied to the non-linear model. Thus, the analysis will be mostly based on the non-linear model, but the linear model will be

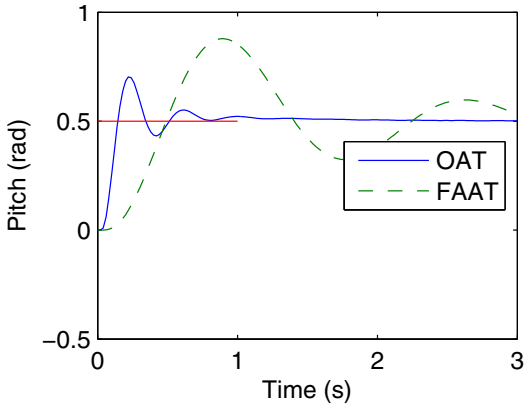

Fig. 8: OAT and FAAT response to a step input with a tuned PD controller and the non-linear model.

used as a basis for controller tuning and root-locus analysis.

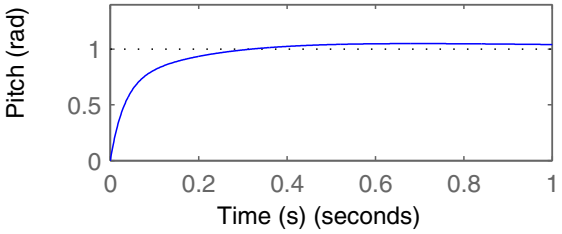

Fig. 9: PD controller with the linear bicopter model

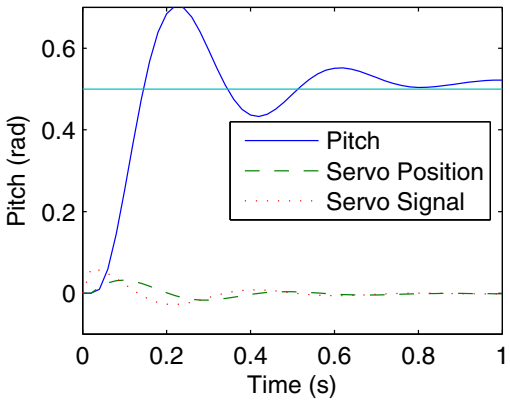

Fig. 10: PD controller with the non-linear bicopter model

The pitch response in Fig. 9 has a very sharp slope for $t = 0$ to $t = 0.1$ which created numerical errors and instability during implementation. The very fast pitch change is possible due to the gyroscopic moment of the bi-rotor. Fig. 10 shows the simulation of the same controller applied to the non-linear model. The saturation of the servo speed clearly shows a less steep rise time, but with significant overshoot.

B. Lead compensator

Following the PD controller design, a lead compensator was developped to obtain less overshoot and a faster convergence. Compensators improve phase response and are very fast when implemented, which is an important criteria for implementation on a low power microcontroller. The lead compensator introduces a pair of pole and zero. It has the form:

$$C(s) = K\frac{s+r}{s+p} \tag{21}$$

Fig. 11 shows the result of the simulation of the lead compensator applied to the linear model and Fig. 12 shows the same simulation using the lead compensator applied to the non-linear model. The constants for all the controllers used are shown in Table II. The linear and non-linear models behave in a similar manner, but the latter showed more overshoot. The higher overshoot seen in the non-linear simulation is partly due to the larger time-step used for the simulations, which is an additional limitation of the micro-controller.

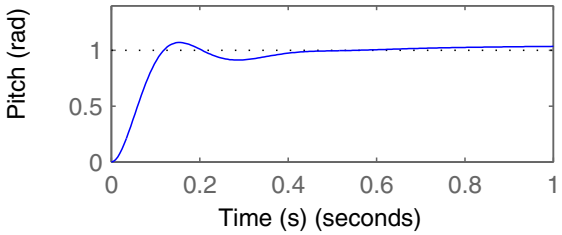

Fig. 11: Lead compensator with the linear model

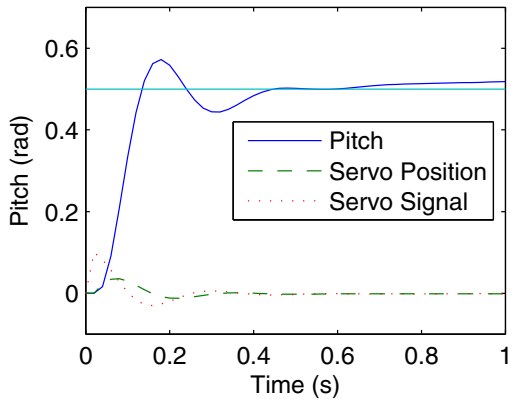

Fig. 12: Lead compensator in Simulink

C. Stability analysis

First, the stability of the open loop is analysed with respect to a gain K with the root locus. Since the branches of the locus remain on the left side of the plane, the system is stable for all gain values. Both the PD and Lead controller have a similar open loop response as seen in Fig. 15.

TABLE II: Controller constants

Constant	Value
P of the FAAT controller	0.02
D of the FAAT controller	0.01
P in the PD controller	0.07
D in the PD controller	0.01
K in the Lead controller	0.09
r in the Lead controller	2
p in the Lead controller	10

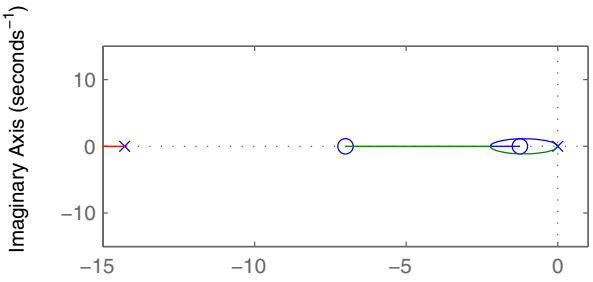

Fig. 13: Root locus for the PD controller

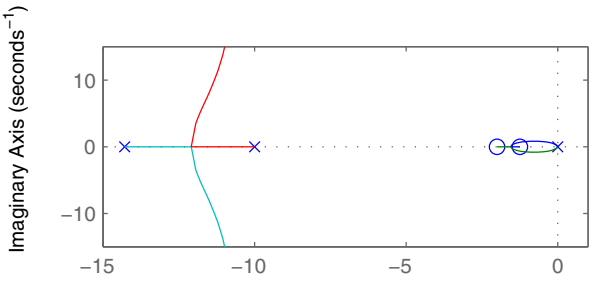

Fig. 14: Root locus for the Lead controller

However, the lead controller adds additional branches on the left of the complex plane.

Torque disturbances from aerodynamic effects, modeling inaccuracy, and mechanical vibrations are also applied on the bi-rotor. The controller should be robust in the face of those disturbances. For an input of zero and a disturbance $D(s)$, the block diagram of the system is shown in Fig. 16.

The transfer function of the response of the bi-rotor to disturbances D(s) is:

$$\frac{\theta(s)}{D(s)} = \frac{1}{1 + C(s)S(s)B(s)} \tag{22}$$

The Bode plot of the transfer function shows that the PD controller is slightly better at rejecting disturbances, as seen in Fig. 17.

However, as seen earlier, the linear model is not accurate to simulate the bi-rotor. Therefore, the response of the bi-rotor to a disturbance will be simulated using the non-linear model. To achieve this in Simulink, the non-linear model

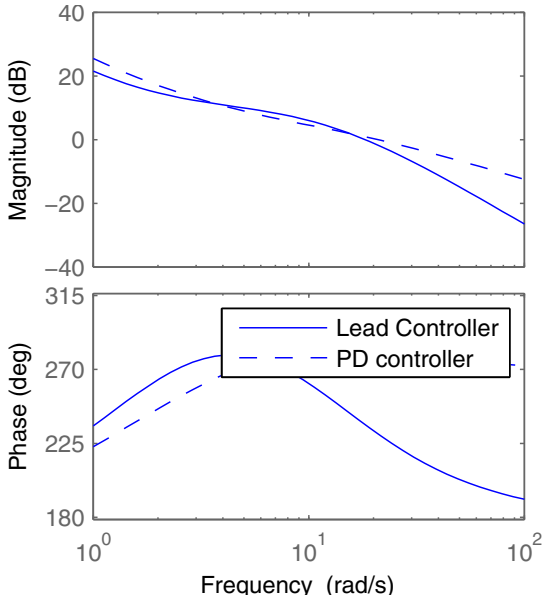

Fig. 15: Open loop response of the Lead and the PD controller

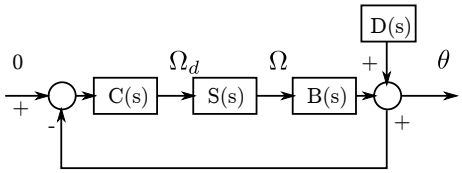

Fig. 16: Pitch response to disturbances

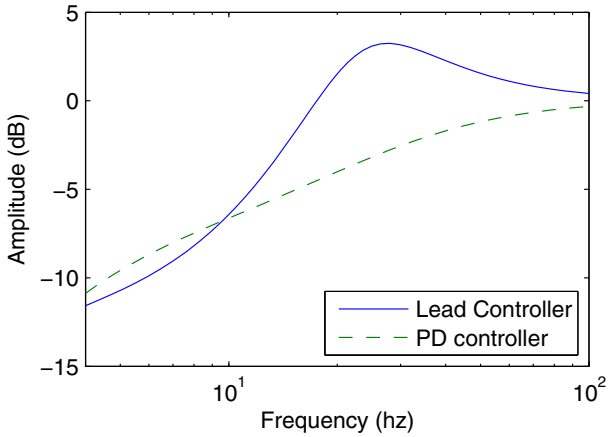

Fig. 17: Bode plot of the pitch response to disturbances using the linear bicopter model

shown before was modified to have the user input set to zero and a pitch disturbance. This disturbance of 0.5 rad amplitude has the form of:

$$D(t) = 0.5\cos\left(\left(\omega_i + \frac{\omega_f - \omega_i}{T_s}\right)t\right) \qquad (23)$$

where T_s is the time the signal disturbance will take to go from its initial frequency ω_i to its final frequency ω_f. The pitch response is simulated and its envelope is calculated. The envelope is the magnitude of the Hilbert transform of the signal. Fig. 18 illustrates the pitch response in the time domain, along with its envelope for the PD controller. The simulation was also performed over 1000s.

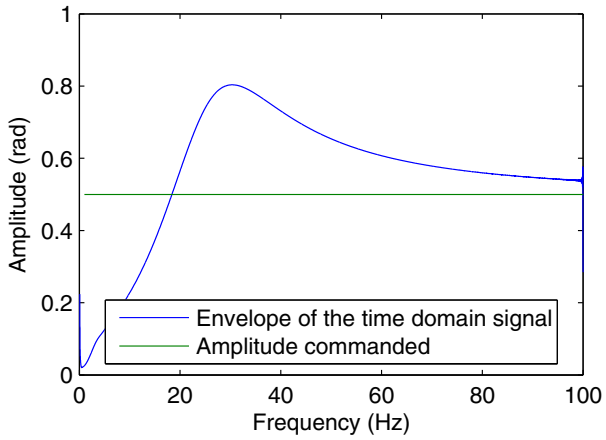

Fig. 18: Pitch response of bi-rotor to D(t) in the time domaine and its envelop when using the PD controller

Time domain result of the disturbance response for both the PD and the Lead controller are then converted to the more typical representation on a Bode plot in Fig. 19. The Bode plot shows that the lead compensator has a slightly higher disturbance rejection for frequencies under 4.5 Hz.

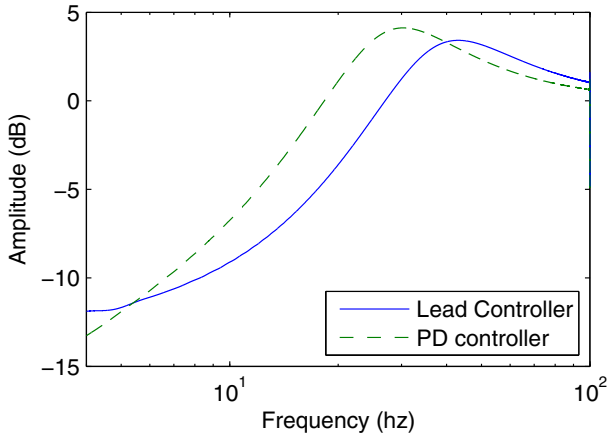

Fig. 19: Bode plot of the pitch response to disturbances using the non-linear bicopter model

IV. Experimental Study

The bi-rotor is controlled by an 8-bit Atmega 32u4 micro-controller. The chip handles data reception, sensor reading, data upload through serial port, attitude estimation, data filtering, attitude control, and PWM generation. The code directing those operations for the experiment is the open source MultiWii 2.2 with a modified control code.

The frame was 3D printed using laser sintering plastic PA2200 and weights 9g. Most walls are 1mm thick to limit deflection. See Fig. 1 and 21 for an overview of the device used. The servos are high torque HS-45HB and the arm is made of a 3D printed motor mount on a carbon shaft. The shaft is supported by two bearings to minimize friction. The device runs on a single 2s 300mAh li-po battery. Both propellers are 5x3 APC on a Turnigy C1826 motor. The electronic speed controllers (ESCs) are 10A Turnigy. The connectivity between the components is shown in Fig. 20. The battery used is 7.4V, but the servo and the controller need lower voltage. Thus, the ESCs also provide 5V from which the power for other components is taken.

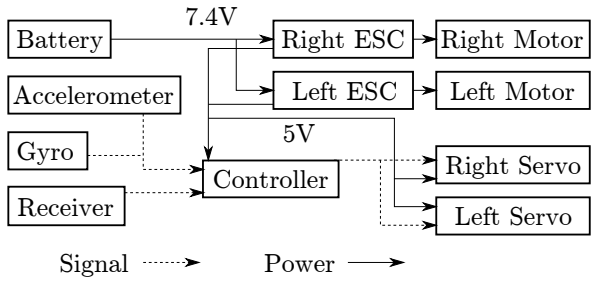

Fig. 20: Diagram of the electrical components

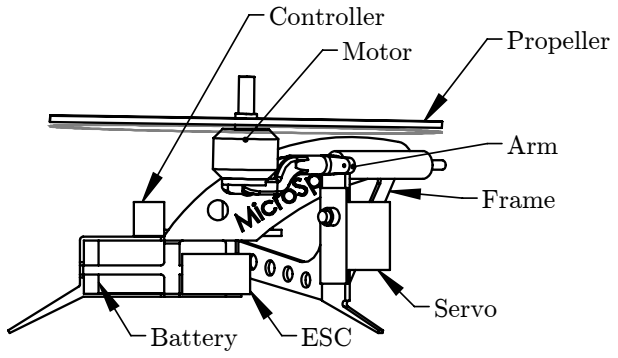

Fig. 21: Side view of the bi-rotor built

A. Numerical implementation of the lead controllers

This section will describe the numerical implementation of the lead controller. In general, numerical implementation of a controller will produce a result different from the analogue implementation. To obtain a discreet version of a controller in the Laplace domain, we need the integral:

$$y(t) = \int_0^t u(t)dt \tag{24}$$

The integral in the controller is approximated by:

$$y_{t+1} = y_t + \Delta t \cdot u_{t+1} \tag{25}$$

Where u_{t+1} is the signal at the next time step, Δt is a suitably chosen time-step, y_t is the previous value of the output, and y_{t+1} is the new calculated value of the integral. In the Laplace domain, the integral is

$$\frac{Y(s)}{U(s)} = \frac{1}{s} \tag{26}$$

By taking the z transform of (25), we obtain:

$$zy(z) = y(z) + z\Delta t \cdot u(z) \tag{27}$$

$$\frac{y(z)}{u(z)} = \frac{z-1}{z\Delta t} \tag{28}$$

By comparing (26) and equation 28, we identify that s can be replaced by $\Delta t/(z-1)$. For a controller of the form:

$$\frac{O(z)}{I(z)} = K\frac{s+r}{s+p} \tag{29}$$

where I is the input of the controller and O is the output, we can replace the s by its equivalent in the z domain and obtain:

$$\frac{O(z)}{I(z)} = K\frac{\frac{z\Delta t}{(z-1)} + r}{\frac{z\Delta t}{(z-1)} + p} \tag{30}$$

Or equivalently

$$I(z) \cdot (z\Delta t + p(z-1)) = KO(z) \cdot (z\Delta t + r(z-1)) \tag{31}$$

Going back to the discrete form:

$$I_k \cdot (-p) + I_{k+1}(p + \Delta t) = K(O_k(-r) + O_{k+1}(r + \Delta t)) \tag{32}$$

We can isolate O_{k+1} and obtain:

$$O_{k+1} = \frac{I_k \cdot (-p) + I_{k+1}(p + \Delta t) + KO_k r}{K(r + \Delta t)} \tag{33}$$

The constant values can be calculated and the equation written as

$$O_{k+1} = LI_k + MI_{k+1} + NO_k \tag{34}$$

The implementation was done on the 8-bit micro-controller, which required using integer arithmetic on 16 or 32-bits values for speed of calculation. Care had to be taken to not lose precision in the calculations and also to prevent the values from overflowing, such as after a multiplication. On the MultiWii platform, this was achieved by modifying the control code.

The test were done by an experienced human pilot. The testing setup includes data acquisition, the bi-rotor, and the transmitter, as shown in Fig. 22.

The values calculated from the simulation were used as a guess for tuning the PID and the lead controllers. Initial test results demonstrated high levels of vibrations, even without any dynamic control inputs. The frame showed deformations around the servo mounts, which translated in an uncontrolled $\pm 2.5^\circ$ rotation of the arms (Ω_l and Ω_r). The lead controller showed improvements over the PD controller, but more experimental tests are needed with longer flight time. The test platform demonstrated the need for:

- Balanced motors.

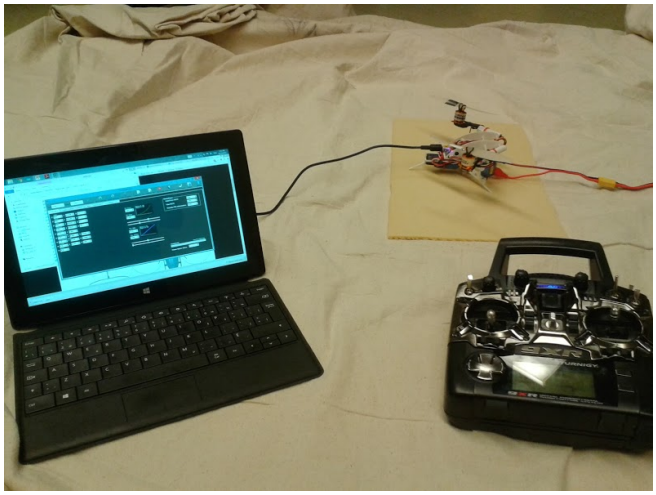

Fig. 22: Computer, bi-rotor and transmitter used for testing.

- More rigid transmission between the servos and the arms
- Increased the rigidity of the frame and of the links.

V. Conclusion

In summary, this paper presented a detailed model of a bi-rotor with oblique arms, which, to the knowledge of the author, has not previously been studied theoretically or experimentally. A faster pitch response for OAT compared to FAAT, due to the gyroscopic torque, was demonstrated. Also, a PD and a lead controller were studied in simulation, with a non-linear model for the pitch control of the bi-rotor. The lead controller demonstrated faster pitch response and better stability compared to the PD controller. The stability of both controllers was studied. Finally, an OAT design was proposed and preliminary experimental observations were recorded. The full implementation of the controller remains a topic of future research.

References

[1] H. Wu, M. Lv, C. Liu, and C. Liu, "Planning efficient and robust behaviors for model-based power tower inspection," in *Applied Robotics for the Power Industry (CARPI)*, Zurich, 2012, pp. 163–166.

[2] J. Escareno, A. Sanchez, O. Garcia, and R. Lozano, "Triple tilting rotor mini-UAV: Modeling and embedded control of the attitude," *2008 American Control Conference*, no. 1, pp. 3476–3481, Jun. 2008.

[3] Y. Long and D. J. Cappelleri, "Omnicopter: A Novel Overactuated Micro Aerial Vehicle," in *Advances in Mechanisms, Robotics and Design Education and Research*, V. Kumar, J. Schmiedeler, S. V. Sreenivasan, and H.-J. Su, Eds. Springer International Publishing, 2013, ch. 16, pp. 215–216.

[4] Starlino, "Introduction & Demo of the QuadHybrid Design," 2012. [Online]. Available: http://www.starlino.com/quadhybrid_intro.html

[5] M. Cutler, N. K. Ure, B. Michini, and J. P. How, "Comparison of Fixed and Variable Pitch Actuators for Agile Quadrotors," in *AIAA Guidance, Navigation, and Control Conference (GNC)*, Portland, OR, Aug. 2011.

[6] C. Youngblood, "Stingray 500," 2013. [Online]. Available: http://curtisyoungblood.com/V2/content/about-curtis

[7] A. Fabio, "Quadcopters Go Inverted by Reversing Their Motors," 2013. [Online]. Available: http://hackaday.com/2013/11/26/quadcopters-go-inverted-by-reversing-their-motors/#more-108392

[8] J. Verbeke, "The Design and Construction of a Novel High Endurance Compound Multicopter," in *UVS Tech edition*, Moscow, 2013.

[9] S. Driessens and P. Paul E. I., "Towards a More Efficient Quadrotor Configuration," in *IEEE/RSJ International Conference onIntelligent Robots and Systems (IROS)*. Tokyo: IEEE, 2013.

[10] C. P. Coleman, "A Survey of Theoretical and Experimental Coaxial Rotor Aerodynamic Research A Survey of Theoretical and Experimental Coaxial Rotor Aerodynamic Research," NASA, Ames Research Center, Moffet Field, California, Tech. Rep. March, 1997.

[11] G. Gress, "Using Dual Propellers as Gyroscopes for Tilt-Prop Hover Control," in *Biennial International Powered Lift Conference an Exhibit*. Williamsburg: AIAA, 2002. [Online]. Available: http://arc.aiaa.org/doi/abs/10.2514/6.2002-5968

[12] F. Kendoul, I. Fantoni, and R. Lozano, "Modeling and Control of a Small Autonomous Aircraft Having Two Tilting Rotors," *IEEE Transactions on Robotics*, vol. 22, no. 6, pp. 1297–1302, 2006.

[13] C. Papachristos, K. Alexis, and A. Tzes, "Design and experimental attitude control of an unmanned Tilt-Rotor aerial vehicle," *2011 15th International Conference on Advanced Robotics (ICAR)*, pp. 465–470, Jun. 2011.

[14] P. Castillo, A. Dzul, and R. Lozano, "Real-time stabilisation and tracking of a four rotor mini-rotorcraft," *IEEE Transactions on Control Systems Technology*, pp. 510 – 516, 2004.

[15] A. Bemporad and C. Rocchi, "Decentralized linear time-varying model predictive control of a formation of unmanned aerial vehicles," *IEEE Conference on Decision and Control and European Control Conference*, pp. 7488–7493, Dec. 2011.

[16] M. S. Selig, "Modeling Propeller Aerodynamics and Slipstream Effects on Small UAVs in Realtime," *AIAA Atmospheric Flight Mechanics Conference*, no. August, pp. 1–23, 2010.

[17] T. Wada, M. Ishikawa, R. Kitayoshi, I. Maruta, and T. Sugie, "Practical modeling and system identification of R/C servo motors," in *Control Applications, (CCA) Intelligent Control, (ISIC), 2009 IEEE*, 2009, pp. 1378–1383.